



Trace double-component gas sensor in photoacoustic spectroscopy based on frequency division multiplexing

Hao Zhang¹ · Cunwei Tian¹ · Zongliang Wang¹ · Xiukun Zhang¹

Received: 18 December 2018 / Accepted: 23 July 2019 / Published online: 30 July 2019
© Springer Science+Business Media, LLC, part of Springer Nature 2019

Abstract

In this paper, we demonstrated a trace double-component gas detection system based on frequency division multiplexing using two-way distributed feedback laser diode (DFB-LD) as the excitation laser source. In the frequency response range of photoacoustic spectroscopy (PAS) cell, this detection system could detect the second harmonics of different frequencies f_0 and f_1 , which were excited by the gas absorption using the two wavelengths of DFB-LD at modulation frequencies $f_0/2$ and $f_1/2$. Unlike previous double-component gas sensor, these two DFB-LDs connected into the both ends of PAS cell without optical fiber coupler could effectively improve the excited light intensity and simplify the system structure. This feature allowed the trace detection of double-component gas of mixed-methane (CH_4) and water (H_2O) vapor with a low detection limits 11.055 ppm and 885 ppb, respectively. Additionally, the linear responses to the gas concentration were achieved 0.9986 and 0.9997, and it exhibited potentially as an effective detection system for complex gas component.

Keywords Double-component gas detection · Photoacoustic spectroscopy · Two-way distributed feedback laser diode · Frequency division multiplexing

1 Introduction

The detection and quantification of trace chemical species in gas phase has become an important topic of research interest, especially in applications such as medical diagnostics (Kosterev et al. 2005), gas chemical reactions process (Dong et al. 2014), environmental monitoring and noninvasive exhaled breath analysis (Hodgkinson and Tatam 2013; Zhang et al. 2018). However, with the increasing complexity of the operational environment, the detection of one single gas was no longer meets needs of actual detection. For example, aerospace and military fields have put forward higher requirements for multi-components gas sensor, such as the successful launch of the Tiangong 2, the Shenzhou eleven spacecraft, which needs safer and more accurate detection system to guarantee the safety of

✉ Cunwei Tian
tiancw2008@163.com

¹ School of Physics Science and Information Technology and Shandong Key Laboratory of Optical Communication Science and Technology, Liaocheng University, Liaocheng 252059, China

equipment and personnel. To date, it is difficult to ensure the reliability and stability of the dual-gas sensor, which depends on separate system when environmental monitoring or controlling gas chemical reactions requires simultaneous detection of multi-components (Cui et al. 2018; Li et al. 2018). Therefore, there are urgent needs to design and fabricate multi-components detection system.

PAS technology to detect a weak photoacoustic signal in a gas medium has proven to be an attractive solution for selective and sensitive detection and quantification of molecular trace gas since its invention (Triki et al. 2015; Liu et al. 2016). To realize multi-components detection, various fiber sensors based on Raman spectra (Li et al. 2008), multi-band laser and quantum cascade laser were used to detect mixed component. Cumis et al. (2014) reported a new detection system, which can detect the Hydrogen sulfide (H_2S) concentration limit of 450 ppb in the mixture of nitrogen (N_2) and H_2S . Wu et al. detected two gas concentrations by focusing two beams of two independently modulated lasers at two different locations in custom Quartz tuning fork (QTF) (Wu et al. 2017). Ma et al. adopted distributed feedback quantum cascade laser to achieve the detection of carbon monoxide (CO) and nitrous oxide (N_2O), the minimum detection limits reached 1.5 ppb and 23 ppb (Ma et al. 2013). Jahjah et al. (2014) realized the detection of CH_4 and N_2O gases by means of quantum cascade laser, and their sensitivity reached the level of ppb. However, the QTF with a half wide frequency response (only 4 Hz), which made it difficult to detect dual-component gas based on FDM. The high price of quantum cascade laser and the extremely complex technical difficulty of custom QTF all made it uncompetitive in the detection of dual-component gas sensor based on FDM.

The trace double-component gas detection system was developed on the optical fiber sensing application to detect the acoustic vibration originated by absorption of the modulated laser radiation (Miklós et al. 2001; Rey and Sigrist 2007). In this paper, we reported a novel double-component gas sensor using FDM technology and demonstrate its capability for trace detection and differentiating of various gas molecules. Compared with traditional PAS method, our detection system uses unique FDM double-laser source as the excitation signal and microphone to detect acoustic signals. Furthermore, the signal-to-noise ratio (SNR) (Sim et al. 2017) and stability of our double-component gas sensor was effectively improved and the attenuation of laser power was reduced comparing with the 1×2 optical fiber coupler. This gas sensor has several advantages such as structural simplification, low cost, high accuracy and long-term stability. To explore its potential in practical application, the novel gas sensor was employed in label-free detection and differentiation of CH_4 and H_2O vapor, which made it a promising highly sensitive sensor for gas sensing.

2 Theoretical analysis

Photoacoustic effect is a continuous attenuation process of energy in PAS cell, which is a core to complete energy transition of light-thermal-acoustic signals and improve the acoustic signal. Figure 1 showed the schematic diagram of the PAS cell (Wang et al. 2017). It consisted of a cylindrical resonator to enhance the second harmonic signal (the second harmonic signal frequency was $2f$ and the modulation frequency was f) of photoacoustic signal in the middle of PAS cell. Buffer reduced the interference of the related signal at both ends of resonator. The microphone under the resonator was set at the antinode of the acoustic wave, and it was used for monitoring the maximum value of the acoustic signal (Miklós 2015; Wilcken and Kauppinen 2003; Wu et al. 2015). The inlet and outlet of gas

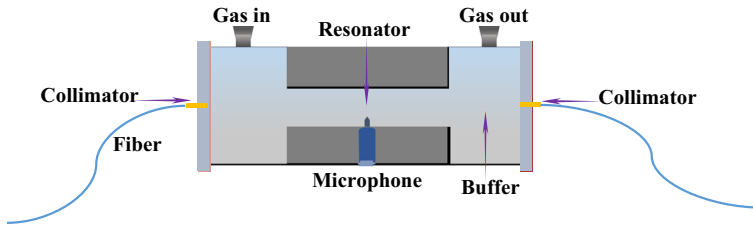


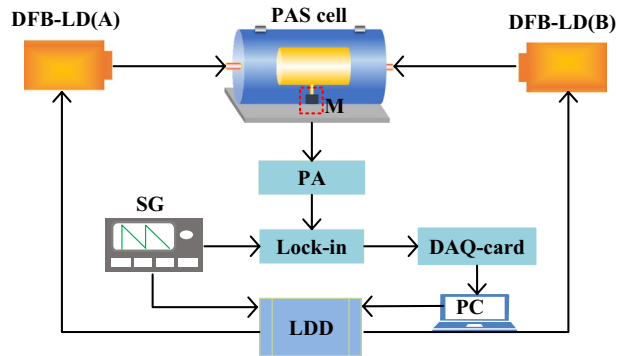
Fig. 1 Schematic diagram of the PAS cell. Position of the gas in, gas out, collimator and microphone were fixed; connect fiber to the collimator of the ends of PAS cell without optical fiber coupler; the buffer was arranged at the end of the resonator and connected to 'gas in' and 'gas out'; output photoacoustic signals were collected using a high-sensitive microphone

were located at the junction of the acoustic wave, which can effectively immunize the impact of the opening of the PAS cell. In recent years, traditional PAS technology based on microphones has developed with the advent of highly sensitive microphones and high-quality PAS cells. It not only greatly improved the detection accuracy and reliability, but also reduced the technical difficulties of multi-component gas concentration detection to some extent. The application of resonator helps us avoid the complex independent resonance structure and laser alignment. The two-way laser modulated with different frequencies could be absorbed by the gases and generated photoacoustic signal. The photoacoustic signal was detected by the microphone (made in Knowles, model: EK-23029-000, sensitivity: -50 dBA, and frequency: 5.2 kHz) and converted into the current. Thereafter, the current was transformed into the voltage signal through the pre-amplifier circuit and the signal was demodulated by the lock-in amplifier (2 Input Channels, 2 Signal Outputs, demodulate both signals at the same time and made from Zurich Instruments, model: HF2LI, frequency resolution: 0.7 uHz), which was connected to different demodulation frequencies (f_0 and f_1 , the modulation frequency was $f_0/2$ and $f_1/2$). The demodulated signal has been collected by the data acquisition (DAQ) card and sent to the computer to determine the second harmonic peak-value (Wang et al. 2017). Finally, the actual concentration was derived from the linear relation between the second harmonic peak-value and the concentration of the gases.

3 Experimental setup

The experimental setup employed was schematically shown in Fig. 2. PAS cell was 80 mm long and 21.2 mm in diameter with a resonant of 34 mm long and 3.2 mm in diameter. Signal generator generated the sinusoidal wave with frequency $f_0/2$ and $f_1/2$ and square wave signals with frequency f_0 and f_1 to obtain the modulation signal of the laser connecting the LDD and demodulation signal of the Lock-in. The DFB-LD(A) (made in Wuhan 69 Sensing Technology Co. LTD; 14 needle butterfly encapsulated laser; the test data of side mode suppression ratio: 42 dB; and the fiber optical power: > 10 mW) with the wavelength of 1370 nm (The test data of wavelength: 1368 nm), and The DFB-LD(B) with the wavelength of 1653 nm were connected to PAS cell respectively without fiber coupling. The photoacoustic signal was detected through a commercial microphone, then the electrical signal was entered PA, Lock-in, DAQ-card and PC in turn.

Fig. 2 Diagram of trace double-component configuration laboratory bench: (DFB-LD) distributed feedback laser diode (PAS cell) photoacoustic spectroscopy cell (M) microphone (PA) pre-amplifier (Lock-in) lock-in pre-amplifier (SG) signal generator (DAQ-card) data acquisition card (LDD) laser diode driver (PC) personal computer

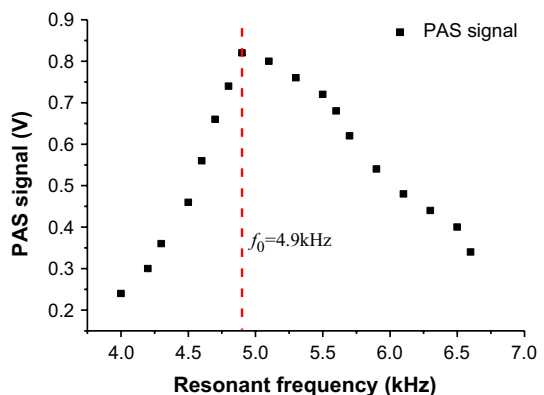


To obtain optimal photoacoustic signal amplitude, the laser wavelength was modulated at the dynamic frequency f (the ranges of 2–3.5 kHz), and derive second harmonic of photoacoustic signal from multiple resonant frequencies. Then to verify the effect of FDM, we used two different modulation frequencies (the DFB-LD(A) modulation frequency was $f_0/2$, The DFB-LD(B) modulation frequency was $f_1/2$) to detect the same gas (H_2O vapor). Finally, two modulation frequencies of stronger second harmonics of photoacoustic signals were selected without frequencies aliasing. To confirm the actual effect of double-component gas sensor detection system, we measured five concentration of (CH_4 and H_2O vapor) gases (400 and 500 ppm, 1060 and 670 ppm, 1250 and 930 ppm, 1670 and 1090 ppm, 2000 and 1480 ppm), and the linear relationship of the second harmonic signal amplitude with the different gas concentrations was confirmed.

4 Results and discussion

The diagram of the resonance profile of the PAS cell was shown in Fig. 3. The optimal response frequency f_0 was 4.9 kHz. The second harmonic of photoacoustic signal of H_2O vapor with different modulation frequencies were showed in Fig. 4. We can ensure that the second harmonic signals were 1.66 V in Fig. 4a (modulation frequency $f_0/2$ was 2.45 kHz) and 1.31 V in Fig. 4b (modulation frequency $f_1/2$ was 2.5 kHz) at normal atmospheric

Fig. 3 Diagram of resonance profile in different resonant frequency cases. The black points represented the PAS signal amplitude of the same PAS cell with different resonant frequencies; position of the red dashed line represented the PAS response signal at the optimal frequency; the optimal resonant frequency f_0 was 4.9 kHz



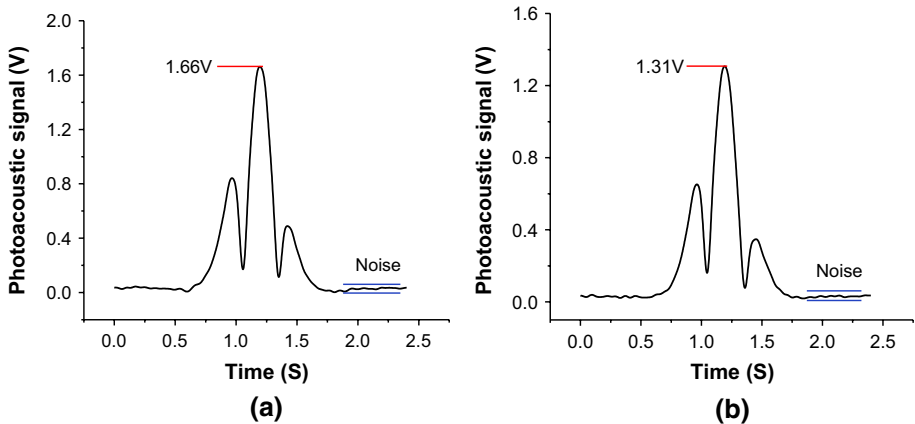


Fig. 4 **a** The black line represented the second harmonic of photoacoustic signal in the case of modulation frequency was $f_0/2$ and laser wavelength was 1368 nm; the red line indicated that the maximum of the second harmonic was 1.66 V. **b** The black line represented the second harmonic of photoacoustic signal in the case of modulation frequency was $f_1/2$ and laser wavelength was 1368 nm; the red line indicated that the maximum of the second harmonic was 1.31 V

pressure. Therefore, the response signals, which were generated by the two-way DFB-LD modulated with different frequencies were different and could be detected by microphone.

Figure 5 depicts the CH_4 and H_2O vapor absorption line in the scope of $5800\text{--}7500\text{ cm}^{-1}$ according to the HITRAN-2004. Two more powerful absorption lines operating at 1368.597 nm for H_2O vapor and 1653.723 nm for CH_4 were employed. The intensities of their absorption lines were 1.8×10^{-20} (molecule cm^{-2}) in 7306.7521 cm^{-1} and 1.46×10^{-21} (molecule cm^{-2}) in 6046.9636 cm^{-1} . The Fig. 6 showed second harmonics of photoacoustic signal of CH_4 and H_2O vapor. We could confirm that the second harmonic amplitudes of CH_4 were 4.40, 3.76, 2.77, 2.43 and 0.90 V (the corresponding concentrations were 2000, 1670, 1250, 1060 and 400 ppm; modulation frequency was 2.5 kHz), and the noise (standard deviation) was 24.37 mV (see the results in Fig. 6a). And for H_2O vapor the second harmonic amplitudes were 4.65, 3.41, 2.92,

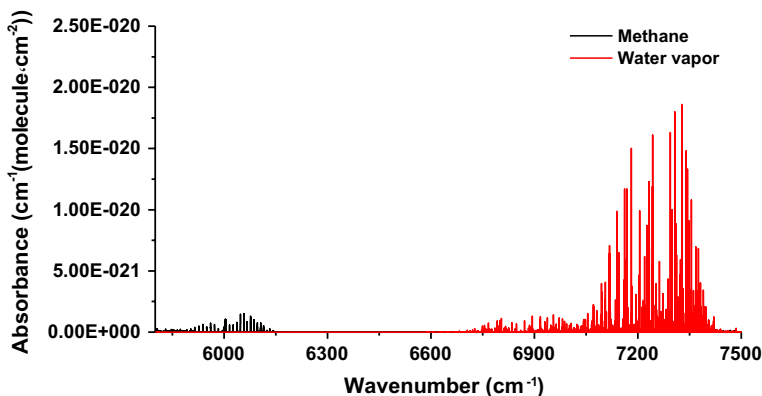


Fig. 5 Water vapor and methane absorption lines in the range of $5800\text{--}7500\text{ cm}^{-1}$

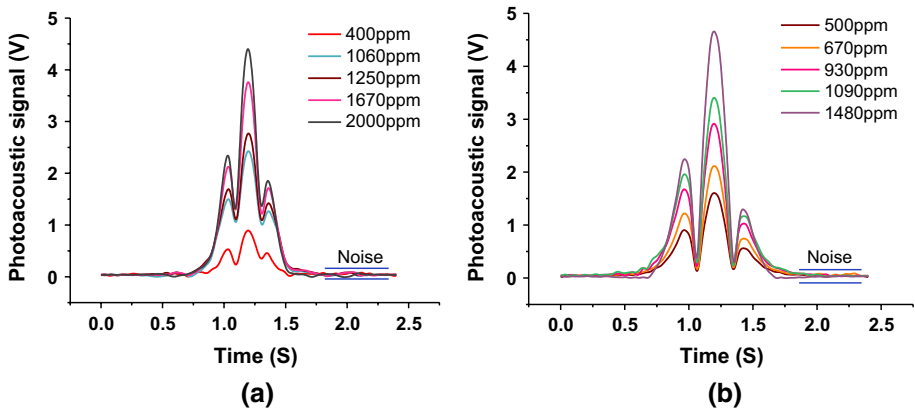


Fig. 6 **a** Methane concentration: 400–2000 ppm; The five color lines represented the second harmonic of photoacoustic signals corresponding to five groups concentration of methane; modulation frequency was $f_1/2$ and laser wavelength was 1653 nm. **b** water concentration: 500–1480 ppm; The five color lines represented the second harmonic of photoacoustic signals corresponding to five groups concentration of water; modulation frequency was $f_1/2$ and laser wavelength was 1368 nm

2.12 and 1.61 V (the corresponding concentration were 1480, 1090, 930, 670 and 500 ppm; modulation frequency was 2.45 kHz), and the noise was 2.78 mV (see the results in Fig. 6b), respectively. The signals diagram of the two gases and their fitting curves were shown in Fig. 7. The acquired data of CH_4 and H_2O vapor yield R-square values, which were 0.9986 and 0.9997, respectively. The minimum detection limits of CH_4 and H_2O vapor were 11.054 ppm and 885 ppb, respectively illustrating an unexceptionable linear response to the gas concentration.

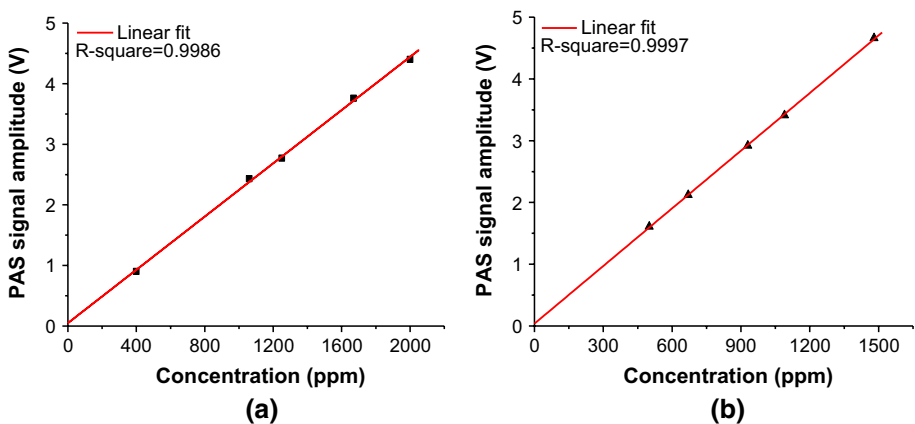


Fig. 7 **a** Second harmonic signal as a function of methane concentration; solid red line was liner least-square fitting to the data points; the quantity R^2 was the coefficient of determination. **b** Second harmonic signal as a function of water vapor concentration; solid red line was liner least-square fitting to the data points; the quantity R^2 was the coefficient of determination

5 Conclusion

We have reported a gas sensor for trace double-component in PAS technology based on FDM. We employed the two-way laser with different wavelengths as the light source to detect the concentrations of two gases at the same time. By mean of FDM, the lasers whose wavelengths corresponding to the absorption peak of the double-component were modulated with different frequencies in the response range of PAS cell. Then, the concentrations of double-component were obtained by their second harmonics acquired by the lock-in amplifier using FDM. The theoretical basis of the scheme was relatively mature and easy to implement, and the system performance was verified by the CH₄ and H₂O vapor. The minimum detection limits of the CH₄ and H₂O vapor were achieved 11.055 ppm and 885 ppb respectively and their R-square values were reached 0.9986 and 0.9997 in the concentration range of 400–2000 ppm and 500–1480 ppm respectively. In summary, the trace double-component gas sensor in photoacoustic spectroscopy based on FDM had superior stability and higher detection precision, simple structure, low manufacturing and maintenance cost, and could be widely used in various fields.

Acknowledgements This work was supported by National Natural Science Foundation of China (61431009).

References

- Cui, X., Dong, F., Zhang, Z., Sun, P., Xia, H., Fertein, E., Chen, W.: Simultaneous detection of ambient methane, nitrous oxide, and water vapor using an external-cavity quantum cascade laser. *Atmos. Environ.* **189**, 125–132 (2018)
- Cumis, M. S. D., Viciani, S., Borri, S., Patimisco, P., Sampaolo, A., Scamarcio, G., De Natale, P., D'Amato, F., Spagnolo, V.: Widely-tunable mid-infrared fiber-coupled quartz-enhanced photoacoustic sensor for environmental monitoring. *Opt. Express* **22**, 28222–28231 (2014)
- Dong, L., Wu, H., Zheng, H., Liu, Y., Liu, X., Jiang, W., Zhang, L., Ma, W., Ren, W., Yin, W., Jia, S., Tittel, F.K.: Double acoustic microresonator quartz-enhanced photoacoustic spectroscopy. *Opt. Lett.* **39**, 2479–2482 (2014)
- Hodgkinson, J., Tatam, R.P.: Optical gas sensing: a review. *Meas. Sci. Technol.* **24**, 1–59 (2013)
- Jahjah, M., Ren, W., Stefański, P., Lewicki, R., Zhang, J., Jiang, W., Tarka, J., Tittel, F.K.: A compact QCL based methane and nitrous oxide sensor for environmental and medical applications. *Analyst* **139**, 2065–2069 (2014)
- Kosterev, A.A., Tittel, F.K., Serebryakov, D.V., Malinovsky, A.L., Morozov, I.V.: Applications of quartz tuning forks in spectroscopic gas sensing. *Rev. Sci. Instrum.* **76**, 1–9 (2005)
- Li, X., Xia, Y., Zhan, L., Huang, J.: Near-confocal cavity-enhanced Raman spectroscopy for multitrace-gas detection. *Opt. Lett.* **33**, 2143–2145 (2008)
- Li, A., Chang, J., Liu, Y., Wang, Q., Wang, Z.: Research on high sensitivity of resonant enhancement laser intracavity photoacoustic spectroscopy technology. *Optik* **156**, 672–676 (2018)
- Liu, Y., Chang, J., Lian, J., Liu, Z., Wang, Q., Qin, Z.: Quartz-enhanced photoacoustic spectroscopy with right-angle prism. *Sensors* **16**, 1–7 (2016)
- Ma, Y., Lewicki, R., Razeghi, M., Tittel, F.K.: QEPAS based ppb-level detection of CO and N₂O using a high power CW DFB-QCL. *Opt. Express* **21**, 1008–1019 (2013)
- Miklós, A.: Acoustic aspects of photoacoustic signal generation and detection in gases. *Int. J. Thermophys.* **36**, 2285–2317 (2015)
- Miklós, A., Hess, P., Bozóki, Z.: Application of acoustic resonators in photoacoustic trace gas analysis and metrology. *Rev. Sci. Instrum.* **72**, 1937–1955 (2001)
- Rey, J.M., Sigrist, M.W.: Differential mode excitation photoacoustic spectroscopy: A new photoacoustic detection scheme. *Rev. Sci. Instrum.* **78**, 1–5 (2007)

- Sim, J.Y., Ahn, C.G., Huh, C., Chung, K.H., Jeong, E.J., Kim, B.K.: Synergetic resonance matching of a microphone and a photoacoustic cell. *Sensors* **17**, 1–10 (2017)
- Triki, M., Ba, T.N., Vicet, A.: Compact sensor for methane detection in the mid infrared region based on quartz enhanced photoacoustic spectroscopy. *Infrared Phys. Technol.* **69**, 74–80 (2015)
- Wang, Q., Wang, Z., Chang, J., Ren, W.: Fiber-ring laser-based intracavity photoacoustic spectroscopy for trace gas sensing. *Opt. Lett.* **42**, 2114–2117 (2017)
- Wilcken, K., Kauppinen, J.: Optimization of a microphone for photoacoustic spectroscopy. *Appl. Spectrosc.* **57**, 1087–1092 (2003)
- Wu, H., Dong, L., Ren, W., Yin, W., Ma, W., Zhang, L., Jia, S., Tittel, F.K.: Position effects of acoustic micro-resonator in quartz enhanced photoacoustic spectroscopy. *Sens. Actuator B Chem.* **206**, 364–370 (2015)
- Wu, H., Yin, X., Dong, L., Pei, K., Sampaolo, A., Patimisco, P., Zheng, H., Ma, W., Zhang, L., Yin, W., Xiao, L., Spagnolo, V., Jia, S., Tittel, F.K.: Simultaneous dual-gas QEPAS detection based on a fundamental and overtone combined vibration of quartz tuning fork. *Appl. Phys. Lett.* **110**, 1–4 (2017)
- Zhang, Q., Chang, J., Wang, F., Wang, Z., Xie, Y., Gong, W.: Improvement in QEPAS system utilizing a second harmonic based wavelength calibration technique. *Opt. Commun.* **415**, 25–30 (2018)

Publisher's Note Springer Nature remains neutral with regard to jurisdictional claims in published maps and institutional affiliations.